PHYSICAL REVIEW B VOLUME 41, NUMBER 6 15 FEBRUARY 1990-II

Molecular-dynamics simulation of amorphous and epitaxial Si film growth on Si(111)

I. Kwon
Ames Laboratory–U.S. Department of Energy and Department of Physics, Iowa State University, Ames, Iowa 50011

R. Biswas
Microelectronics Research Center, Iowa State University, 1925 School Road, Ames, Iowa 50011

G. S. Grest
Corporate Research Science Laboratory, Exxon Research and Engineering Company, Annandale, New Jersey 08801

C. M. Soukoulis
Ames Laboratory–U.S. Department of Energy and Department of Physics, Iowa State University, Ames, Iowa 50011
and Microelectronics Research Center, Iowa State University, 1925 School Road, Ames, Iowa 50011
(Received 6 September 1989)

Both amorphous and epitaxial crystalline Si films have been grown by deposition of Si-atom clusters on a Si(111) substrate with molecular-dynamics simulations utilizing two- and three-body interatomic Si potentials. The amorphous films were produced with deposition conditions that led to low surface diffusion. The *a*-Si films displayed voids, a 15–28 % lower density than *c*-Si, and coordination defects consisting only of undercoordinated atoms with no fivefold-coordinated atoms, in contrast to melt-quenched *a*-Si models. The epitaxial Si(111) growth was achieved under conditions of high surface diffusion consisting of a large initial cluster velocity and moderate substrate temperatures.

I. INTRODUCTION

The development of new semiconductor materials is centrally dependent on film-growth techniques. Amorphous silicon films are commonly deposited with sputtering or glow-discharge methods that involve a "cold" or room-temperature substrate resulting in limited surface diffusion of the deposited species. On the other hand, molecular-beam epitaxy is among the most extensively used techniques for growing high-quality epitaxial films. Recently, Takagi and co-workers[1] have demonstrated that the ionized-cluster-beam (ICB) technique is a viable deposition technique for growing epitaxial Si films and even for *a*-Si films. In the ICB technique atomic clusters are generated by an adiabatic expansion of condensed vapor atoms through a nozzle into a high vacuum region. The clusters are positively ionized by an electron beam, and accelerated towards the deposition surface.

The ICB process is characterized by the charged deposition species as well as a control over the incident kinetic energy of the cluster. Generally epitaxial films can be grown at lower substrate temperatures with the ICB method than with other techniques. A recent ICB study of Ge growth[2] found amorphous Ge film growth at the low substrate temperature of 200 °C but good quality epitaxial growth when the substrate temperature was raised to 400 °C. Indeed substrate temperatures in the range around 200 °C are typical for *a*-Si growth with sputtering, glow-discharge methods, or even ICB methods.

Many aspects of the ICB growth techniques are not well understood, and with a view to understanding these, we perform a simulation of the Si film growth with cluster-beam deposition in this paper. In our previous work[3] we characterized the sensitivity of the spreading of clusters and surface diffusion of the deposited species to the deposition conditions, i.e., incident cluster velocity, cluster temperature, substrate temperature, and cluster size. We identified a range of growth conditions that led to large spreading of the incident clusters. Based on these results we perform simulations in this paper of both amorphous and epitaxial crystalline film growth by choosing the deposition conditions of either low or high surface diffusion, respectively.

We have extensively analyzed the structural characteristics of *a*-Si film that we have obtained with our simulations. There has been much recent activity in the development of *a*-Si models with molecular dynamics.[4–7] In all cases quenching of a melt of bulk Si with periodic boundary conditions was used to generate the amorphous phase. These molecular-dynamics studies have utilized the Stillinger-Weber[8] and the Tersoff[9] model, as well as the Biswas-Hamann[10] model for the interatomic Si potentials. The structural models exhibit root-mean-square (rms) bond-angle distortions between 10° and 14°, rms bond-length variations of about 2%. The vibrational densities of the states compared very well with experiment for both the transverse-acoustic and transverse-optic peaks. A new feature of these models is the presence of coordination defects consisting primarily of threefold- and fivefold-coordinated Si atoms. In fact, the fivefold-coordinated Si atom or floating bond was proposed by Pantelides[11] to be a novel intrinsic defect in *a*-Si and a-Si:H that could account for various ESR and H-diffusion measurements. Either fivefold-coordinated

 ©1990 The American Physical Society

atoms were the only or majority defects[4,5] or there were both threefold- and fivefold-coordinated sites in comparable numbers[6] in the various molecular-dynamics simulations.

A drawback of the *a*-Si models discussed to date is that the melt-quenched process by which they are generated is in many ways different from the experimental growth process of deposition on a cold substrate by which all amorphous Si films are commonly grown. In fact, Phillips[12] has observed that the kinetics of the growth from a vapor phase should not favor overcoordination defects, but favor undercoordination defects instead. In this paper, we systmatically compare the properties of the deposited *a*-Si models with the bulk melt-quenched models and identify important differences between these two classes of models. This is the motivation of the present work. This has important consequences both for the floating-bond hypothesis and for evaluating the previous *a*-Si models themselves.

Another aspect studied in this paper is the voids in amorphous materials. Previously, approximate spherical voids of various sizes were introduced into the bulk *a*-Si models by removing shells of atoms and allowing the system to fully relax.[13] The structure factor $S(q)$ of these void structures displayed a rapid rise for wave vctors q less than 1 Å^{-1}, similar to the Guinier scattering observed experimentally.[14] In these deposition studies we also find voids in the *a*-Si layers and this allows us to compare these void structures to our previously obtained void structures. Recently, Landman and Luedtke[15] have reported the growth of *a*-Si layers by depositions of single atoms using the Stillinger-Weber potential.[8] In their simulations,[15] microvoids in the *a*-Si layers were obtained when the impinging atoms were incident at random directions to the substrate, whereas a columnar film microstructure was found for a beam directed at 60° from the normal to the substrate.

In Sec. II of this paper we demonstrate that the cluster deposition can lead to epitaxial growth. We have chosen deposition conditions that lead to large surface diffusion of the deposited atoms. To the best of our knowledge this is the first simulation of epitaxial growth from cluster deposition. Prior work by Schneider, Schuller, and Rahman[16] (SSR) using the Stillinger-Weber (SW) potential[8] achieved epitaxial growth on the Si(111) surface by deposition of single atoms. Intermediate substrate temperatures ($T/T_m \sim 0.4$, where T_m is the melting temperature of SW model) were used. Gawlinski and Gunton[17] (GG) have also simulated epitaxial growth on a Si(100) surface with the SW potential[8] and confirmed the presence of an epitaxial temperature below which amorphous growth was found. Although amorphous growth was obtained in both of these above simulations, only a limited analysis of the amorphous layer structure was presented.

A major difficulty exists in comparing results of molecular-dynamics simulations with experiments. Owing to limitations in computer time and the small time step that is used, the molecular-dynamics simulations are typically performed over real-time scales of a few nanoseconds, which are several orders of magnitude smaller than time scales in experiments. Hence, the simulations cannot address long-time dynamical properties such as long-range diffusion of atoms. On the other hand, molecular dynamics with realistic interatomic interactions well describe many aspects of shorter range (and smaller time) relaxations, which as we will see is crucial in describing both epitaxial and amorphous growth.

The computational method and the simulation system is described in Sec. II, whereas the surface diffusivity of the clusters are studied in Sec. III. The amorphous Si film growth is discussed in Sec. IV followed by the epitaxial growth in Sec. V, and a summary in Sec. VI.

II. COMPUTATIONAL METHOD

Although a number of classical models[8,9] for interatomic Si interactions may be equally suitable for simulations of film-growth processes, we have used the Biswas-Hamann model[10] of separable two- and three-body interatomic Si potentials. This model was originally developed by fitting to first-principles total-energy calculations for energies of bulk, surface, and defect Si configurations. A strengthening of the three-body potential by a factor of 2.50 was found to be necessary for describing amorphous silicon in the previous work.[6]

The estimated melting temperature of the original Biswas-Hamann potential is between 0.24 and 0.26 eV, which is somewhat higher than the experimental melting temperature $k_B T_m$ of 0.147 eV. One of the reasons for using this potential is that a number of melt-quenched *a*-Si models were previously generated with this model. These melt-quenching simulations consisted of equilibrating a liquid-Si configuration which was then cooled to generate an amorphous structure. Therefore, deposition simulations with the same model can give a direct comparison of the difference between these two methods. Also, we have already studied[3] the dependence of the surface diffusivity to the deposition conditions with this potential, and these results can be directly utilized in this paper.

The simulation system consisted of four movable Si(111) double layers above two immobile Si(111) double layers that modeled the underlying crystal. A rectangular cell, with dimensions 20.25 and 21.06 Å, consisting of 60 Si atoms per Si(111) double layer, with periodic boundary conditions in the x and y directions was used for the amorphous growth simulations. On the other hand, the epitaxial growth simulations in Sec. V utilized the substrate with a larger area of 96 atoms per Si(111) double layer. An in-plane lattice spacing of 4.05 Å was used for the Si(111) substrate corresponding to the equilibrium value for this Si model. Clusters with center-of-mass velocity v_z towards the substrate were introduced into the system from a large enough height so that they were outside the range of interaction of substrate atoms or previously deposited cluster atoms.

In the molecular-dynamics calculations, Newton's equations of motion have been integrated in time, with the Gear fifth-order predictor-corrector algorithm, for a collection of substrate and deposited Si atoms. The time step (Δt) used in this paper is 0.0037 ps, which is an approximately small fraction of the silicon-optical-phonon

period of 0.0638 ps. In the entire simulation process, the temperature of the substrate is maintained at a constant temperature T_s. In any thin-film growth experiment, heat energy is added to the surface by the deposited species. The thermal conductivity of the substrate allows this heat to be transported into the bulk of the substrate material. In our simulations we model this thermal-conduction process by monitoring the average temperature of movable substrate layers every ten time steps. If this temperature exceeds the desired temperature T_s, the velocities of the atoms in the movable layers are rescaled to maintain a constant T_s. Therefore, the substrate layer acts as a heat reservoir that absorbs heat through collisions with the deposited species. We can increase this energy transfer rate by extending the velocity rescaling to include some of the deposited atoms also, and this has been used in the amorphous growth.

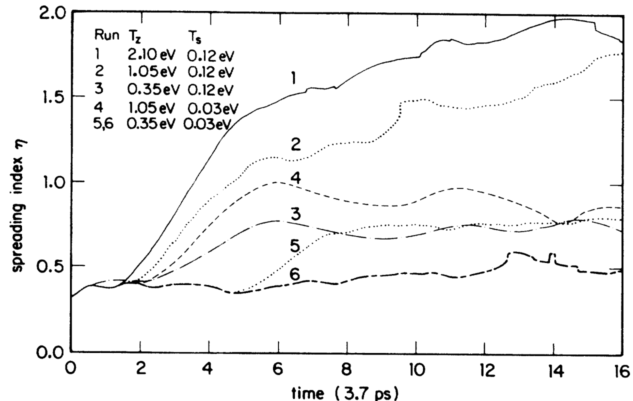

FIG. 1. Time evolution of the normalized spreading index [Eq. (11)] for 33-atom clusters. The deposition conditions, consisting of the cluster translational temperature (T_z), and surface temperature (T_s), were varied in each case.

III. SENSITIVITY OF SURFACE DIFFUSION TO DEPOSITION CONDITIONS

As recognized in previous studies[3,18] an important requirement in growing epitaxial films from cluster deposition is that each impinging cluster should dissociate and spread uniformly on the substrate. Alternatively, if the spreading of the clusters is small, amorphous layer growth is expected. We have previously demonstrated that cluster-beam growth simulations are feasible and require substantially less computer time than simulations with single-atom deposition.[3] The reason is that the adsorbed cluster atoms equilibrate with the substrate more rapidly, allowing the next cluster to be deposited sooner than with single atom deposition. This is because the clusters initially have a considerable amount of binding energy. On adsorption, there is a smaller increase in the binding energy per atom for the cluster than for the single atom case, and consequently less kinetic energy gained (or less heating) for the cluster than the atom.

We explore the parameter space of deposition parameters to define parameter ranges suitable for both amorphous and crystalline growth. It would be computationally unfeasible to simulate fully the growth of a thick film under different deposition conditions, and then differentiate between deposition parameters by examining the structure of the films. Instead we adopt the much simpler procedure of studying the dynamics of deposition of a single cluster under different deposition conditions, to gain insight into the important parameters for the growth process.

To accomplish this, we have studied the dependence of the surface diffusivity to deposition conditions [cluster velocity, cluster temperature, and substrate temperature (T_s)] by calculations of the spreading index $\eta(t)$ under different growth conditions (Fig. 1). As found previously, $\eta(t)$ is a convenient measure of the surface diffusivity of the incident cluster and is defined as the mean-square transverse positions of the cluster atoms relative to the cluster center of mass, and can be written as

$$\eta(t)=\sum_{i=1}^{N}[x_i(t)-x_{\mathrm{c.m.}}(t)]^2+[y_i(t)-y_{\mathrm{c.m.}}(t)]^2 . \quad (1)$$

$x_i(t)$, $y_i(t)$, and $z_i(t)$ are the coordinates of the ith atom in the cluster at time t, whereas $x_{\mathrm{c.m.}}(t)$, $y_{\mathrm{c.m.}}(t)$, and $z_{\mathrm{c.m.}}(t)$ define the dynamical position of the center of mass of the cluster. All calculations were performed with amorphous 33-atom clusters incident on a Si(111) substrate. We[3] have previously estimated an optimum cluster size in the range of 30 atoms for the growth simulations. Consequently, all calculations in this paper utilize amorphous 33-atom clusters.

As demonstrated by the curves 1, 2, and 3 in Fig. 1 the initial cluster velocity is a highly sensitive parameter controlling the surface diffusivity, with the cluster spreading monotonically increasing as the cluster translational temperature (T_z) is increased from 0.35 to 2.1 eV. This temperature T_z is simply the cluster translational kinetic energy. We note from runs 1 and 2 that $\eta(t)$ does not saturate after 16×10^3 time steps (59 ps), i.e., the deposited species is still diffusing on the surface. By allowing the system to run for 32×10^3 time steps (118 ps) we find that $\eta(t)$ does reach an approximately steady-state value (Fig. 2). We identify then that $(30-32)\times10^3$ time steps (111–118 ps) is a suitable length of time to allow for equilibration of the deposited cluster.

The form of $\eta(t)$ (Fig. 1) illustrates the equilibration of the cluster atoms after deposition. During the first 5–6 ps the cluster has not interacted with the substrate and hence η is constant. After 7 ps the cluster reaches the surface and the hot cluster atoms diffuse rapidly on the surfaces as indicated by the sharp rise of $\eta(t)$ with time. The cooling of the cluster atoms leads to gradual slowing down of the $\eta(t)$ following by a steady-state value of $\eta(t)$ where atoms have equilibrated and are no longer diffusing. A longer equilibration time is needed for the higher velocity runs 1 and 2. The initial slope of the $\eta(t)$ curves provides an estimate of the (initial) diffusion coefficient since the center of mass of the cluster is almost constant with time. We find $(3.3,2.1,1.2)\times10^{-4}$ cm^2/s for runs 1, 4, and 3, respectively. These values compare well with both experiment and theoretical estimates[19] and

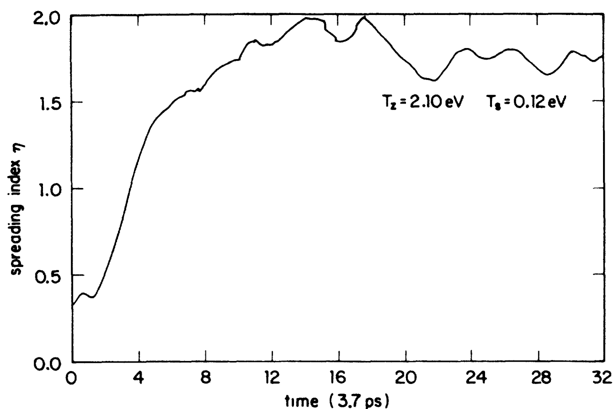

FIG. 2. Time evolution of the normalized spreading index [Eq. (1)] for 33-atom clusters with high translational temperature ($T_z = 2.1$ eV).

are larger than surface diffusivity values calculated[19] for the Stillinger-Weber potential.[8]

In addition, if we retain the high cluster translational temperature T_z of 1.05 eV in run 2, but reduce the substrate temperature T_s from 0.12 to 0.03 eV, the spreading of the cluster is substantially inhibited, as exhibited in run 4, Fig. 1. This illustrates the important coupling between substrate tempratures and cluster velocities. It is, in fact, possible to achieve high surface diffusivity by lowering the substrate temperature, and increasing the incident cluster energy, a trend that is seen in experimental ICB growth studies. The epitaxial growth simulations in Sec. V utilize the deposition conditions in runs 1 and 2, of a moderate substrate temperature (0.12 eV), coupled with high cluster velocities ($T_z = 1.05$ and 2.10 eV).

Alternatively, the amorphous growth simulations in Sec. IV utilize both the low T_z (0.35 eV) and low T_s (0.03 eV) conditions for which the surface diffusivity is small as displayed in run 5 of Fig. 1. Finally, run 6 in Fig. 1 shows the spreading of the cluster on an amorphous substrate with the same deposition parameters as in run 5. As anticipated, the surface diffusivity is further inhibited on an amorphous or rough substrate owing to potential wells on the surface that can trap some of the incident atoms. Run 6 is, in fact, the result for the final (14th) cluster during the growth of the a-Si film in Sec. IV. All the other intermediate desposited clusters have diffusivities in between runs 5 and 6.

We have previously estimated[3] that cluster temperatures did not have a significant effect on the surface diffusivity, and hence keep all cluster internal temperatures at 0.12 eV. The cluster internal temperature is two-thirds of the kinetic energy of the cluster in a comoving reference frame that has the same center-of-mass velocity as the cluster. The clusters have a glassy structure. In order that the results in this section were not biased by a particular cluster structure, we used clusters that were relaxed, equilibrated fragments of bulk a-Si networks that were generated with melt-quenching molecular-dynamics simulations.

IV. AMORPHOUS SILICON FILM GROWTH SIMULATIONS

In this section we utilize the deposition conditions, determined in the preceding section that lead to low surface diffusivity, to simulate the growth of an a-Si film on a Si(111) substrate. These deposition conditions correspond to a low translational energy ($T_z = 0.35$ eV) of the impinging clusters, in conjunction with a cold substrate temperature ($T_s = 0.03$ eV) which are the parameters of run 5 in Fig. 1. Although run 3 of Fig. 1 with a higher substrate tempreature $T_s = 0.12$ eV and the same cluster velocity appeared equally suitable, the higher substrate temperature would lead to greater difficulty in keeping the deposited atoms cool, and hence the T_s of 0.03 eV was chosen. In fact, experimentally substrate temperatures around 0.04 eV are typically used in a-Si film growth.

Following the simulations described in Fig. 1, we chose a deposition rate of one cluster deposition every 20 000 time steps (74 ps). This time seemed adequate to allow the deposited 33-atom clusters to equilibrate with the substrate, at least for the low surface diffusivity conditions.

Two schemes were implemented in cooling the deposited atoms. In the first case, the velocities of only the initial 240 substrate atoms were rescaled to maintain this substrate at a constant temperature T_s of 0.03 eV. The energy transfer rate to the substrate becomes slower as the adsorbate layer grows in thickness, resulting in the adsorbate gradually warming up during the simulation with a temperature gradient existing through the adsorbate. After deposition of 14 clusters (462 atoms) local temperatures varied from ~ 0.05 eV just above the substrate to ~ 0.20 eV at the top surface. After deposition of the last (14th) cluster, the system was allowed to evolve for 48 000 time steps (178 ps), before rescaling the adsorbate velocities to cool the adsorbate temperature to 0.03 eV in a 120 ps run. Finally a steepest descent relaxation led to a zero-temperature amorphous structure we label as $M1$. The total simulation time corresponded to 1.35 ns, i.e., 3.6×10^5 time steps.

In the second scheme the adsorbate was maintained at a much cooler temperature than in the $M1$ simulation, leading to substantially reduced surface diffusion. This was achieved by controlling the velocities of adsorbate atoms that were at least 3.0 Å away from the growing surface. We took care not to control the atoms at the surface so that the growth dynamics at the surface was not affected. As the clusters were deposited we would periodically raise the number of control atoms. The control atoms were maintained at 0.03 eV and were for most of the time more than 3.0 Å below the growing surface. The result of this procedure was to have at the end of the simulation three adsorbate slabs with upper surfaces that were 11.2, 21.4, and 26.9 Å above the structure consisting of 132, 126, and 74 atoms, respectively, that were individually maintained at 0.03 eV.

Up to deposition of the sixth cluster the results of the previous run were used so that the amorphous layers near the substrate in this simulation were identical to $M1$.

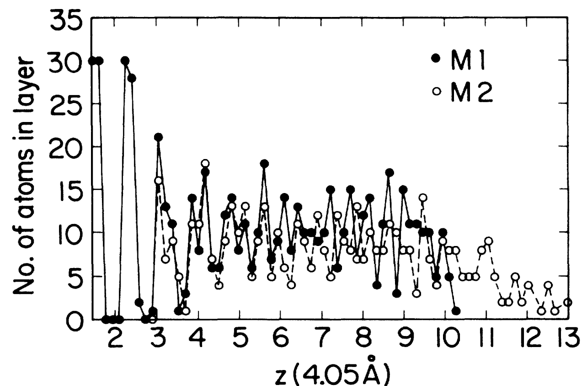

FIG. 3. Variation of the density of deposited atoms in the z direction for the two a-Si layers $M1$ and $M2$. A bin size Δz of 0.65 Å has been used.

The final annealing and steepest descent relaxation were similar to the $M1$ case, leading to the structure $M2$. The total simulation time was 1.08 ns, which required about 250 h of Scientific Computer Systems, Inc. SCS-40 mini-supercomputer central-processing-unit (CPU) time.

The amorphous nature of the deposited layers is displayed by the density of atoms in the perpendicular z direction (Fig. 3). There is a remnant of crystallinity in the adsorbate immediate adjacent to the substrate ($3.0a < z < 3.30a$, $a = 4.05$ Å), but a relatively random distribution for higher z ($z > 4.0a$) where the structure is amorphous. This interpretation is also supported by the projected atomic positions of the first two deposited layers ($z < 4.34a$, or 8.1 Å above the substrate), in Fig. 4. The first amorphous layer reveals a domain of crystalline six-member rings. There is also a void of considerable extent (~8–10 Å laterally) around which distorted five- and eight-membered ring structures exist. For the second deposited layer crystallinity is absent and the structure is amorphous at and above this layer. The crystallinity in the interfacial deposited layer is consistent with the results of SSR (Ref. 16) who also observed a similar effect in their amorphous layer generated with single-atom depositions. It is not surprising that the crystalline substrate induces a ordering directly adjacent to it.

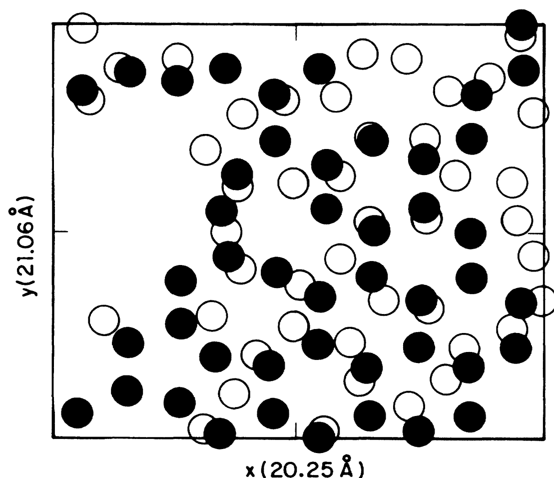

FIG. 4. Projection of atoms of the first two deposited layers in the x-y plane. The first-layer atoms are represented by solid circles.

The radial distribution $g(r)$ of the amorphous layers (Fig. 5) shows considerable short-range order with well-defined first and second neighbor peaks, similar to the $g(r)$ for the melt-quenched a-Si models and the a-Si model generated by Wooten, Weaire, and Winer (WWW) (Ref. 20) from Monte Carlo simulations (Fig. 5). Contrary to a-Si models generated from the Stillinger-Weber potential,[5] and in agreement with experiment,[21] there is no shoulder in the second peak of $g(r)$, and this will be discussed later. There are fewer neighbors in between the first and second peaks of $g(r)$ in the a-Si layers than in the melt-quenched a-Si models. The first peak of $g(r)$ is somewhat sharper and stronger in the WWW model than in either of the molecular-dynamics models.

The bond-angle distribution of the a-Si layers, the melt-quenched a-Si model, and the WWW model is compared in Fig. 6. A bond cutoff of 2.94 Å, in between the first and second peaks of $g(r)$, was used to define bonds.

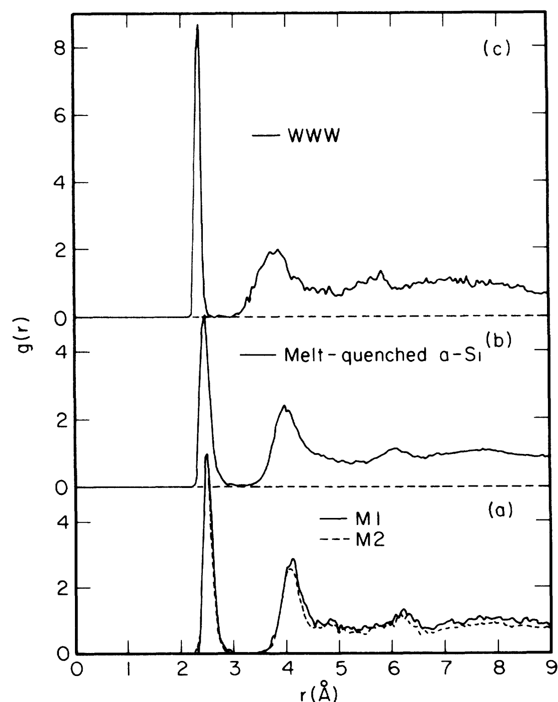

FIG. 5. Pair distribution functions $g(r)$ for (a) amorphous states produced by cluster deposition ($M1$ and $M2$), with all the deposited atoms included, (b) 2000-atom amorphous system produced by melt-quenching of Si atoms (Ref. 6), and (c) the continuous random-network model of Wooten, Winer, and Weaire ($W3$, Ref. 20), generated with Monte Carlo simulations.

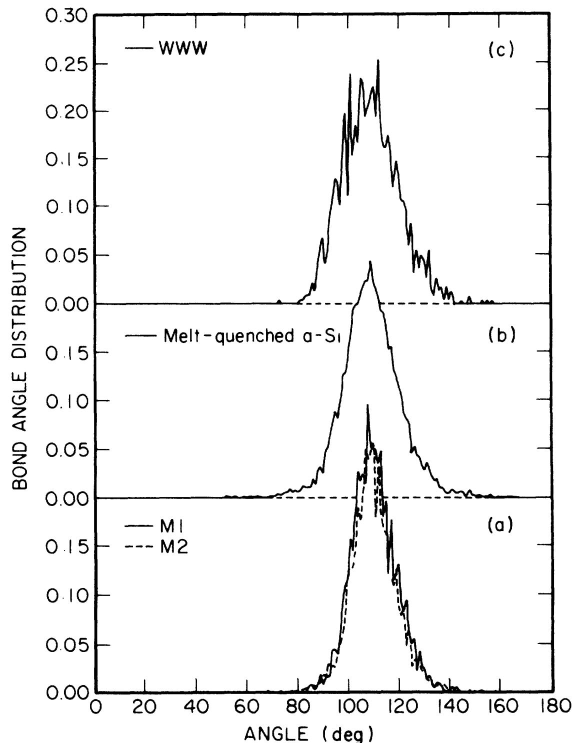

FIG. 6. Bond-angle distributions for (a) amorphous states produced by cluster deposition ($M1$ and $M2$), with all the deposited atoms included, (b) 2000-atom amorphous system produced by melt-quenching of Si atoms (Ref. 6), and (c) the network of Ref. 20.

The bond-angle distribution (Fig. 6) reveals a narrower distribution around the tetrahedral angle for the a-Si layers than either the melt-quenched or the WWW a-Si models. The observation of a narrower second peak of the radial distribution $g(r)$ for the a-Si layers than for the other a-Si models (Fig. 5) is related to the sharper bond-angle distribution for the a-Si layers. The bond-angle rms values range from 8.6° to 9.2° for the $M1$ and $M2$ a-Si layers (Table I). These values are considerably smaller than in previous melt-quenched bulk models where θ_{rms} ranges from 11° to 14°. A reason for this is that the voids in the a-Si layers substantially reduce the local strain as found in our previous work.[13] The crystalline Si(111) substrate also induces a considerable degree of ordering near it as evident from the lower values near the substrate (Table I).

A remarkable result was that there were no five-coordinated defect sites (floating bonds) in the amorphous silicon films. All the coordination defects instead consisted of undercoordinated atoms, primarily three-coordinated atoms (Table II). This is in direct contrast to melt-quenched a-Si models generated with the same interatomic Si potential. These bulk melt-quenched models (with periodic boundary conditions) had 3.1%, 10.1%, and 8.3% of floating bonds in the $N=216$, 512, and 2000 atom a-Si models.

The reason for the dramatic absence of floating bonds is closely related to our previous finding[13] that voids in the bulk a-Si networks reduce the density of floating bonds by almost an order of magnitude. Our interpretation is that the floating bonds can easily migrate from site to site by a bond-switching mechanism proposed by Pantelides.[11] In the presence of either the internal surfaces of voids or the external growing top surface of the amorphous layer, the floating bonds can easily migrate to these surfaces and then recombine with the large number of dangling bonds at these surfaces. This is consistent with the arguments of Phillips[12] that the kinetics of film growth from a vapor phase, and the presence of internal surfaces, should favor undercoordinated rather than overcoordinated defects. We, in fact, find in the intermediate stage of the $M1$ simulation the existence of two to five floating bonds. During the continuation of this simulation these floating bonds probably have diffused to an external or internal surface and annihilated.

In the studies with the Stillinger-Weber potential,

TABLE I. The rms values of the bond-length and bond-angle distributions together with average bond-length and bond-angle values for the different a-Si layers described in the text. The variations with height z (Å) are also displayed.

	R_{av} (Å)	R_{rms} (Å)	θ_{av} (deg)	θ_{rms} (deg)
$M1$ FULL	2.52	0.087	110.18	8.65
$11.1<z<17.6$	2.49	0.073	110.87	7.43
$17.6<z<30.5$	2.53	0.090	110.91	8.61
$M2$ FULL	2.51	0.092	110.34	9.24
$11.1<z<17.6$	2.49	0.073	110.61	7.86
$17.6<z<30.5$	2.52	0.098	110.30	9.80
$A1$ FULL	2.50	0.087	110.52	8.99
$11.1<z<17.6$	2.49	0.078	110.83	8.41
$17.6<z<30.5$	2.51	0.089	110.43	9.26
$A2$ FULL	2.51	0.093	110.72	9.37
$11.1<z<17.6$	2.51	0.085	110.62	8.27
$17.6<z<30.5$	2.52	0.092	110.75	9.75

TABLE II. The number of atoms N_i with coordination i in the different a-Si layers. The variations with height z (Å) are also displayed, including number of atoms N_{tot} and average coordination numbers $\langle N_i \rangle$.

	N_2	N_3	N_4	N_5	N_{tot}	$\langle N_i \rangle$
$M1$ FULL	4	127	331	0	462	3.71
$11.1<z<17.6$	0	39	52	0	91	3.57
$17.6<z<30.5$	0	42	162	0	204	3.79
$M2$ FULL	16	181	265	0	462	3.54
$11.1<z<17.6$	3	35	44	0	82	3.50
$17.6<z<30.5$	4	56	113	0	173	3.63
$A1$ FULL	16	180	266	0	462	3.54
$11.1<z<17.6$	1	37	48	0	86	3.55
$17.6<z<30.5$	3	60	107	0	170	3.61
$A2$ FULL	15	195	252	0	462	3.51
$11.1<z<17.6$	1	35	50	0	86	3.57
$17.6<z<30.5$	1	74	109	0	184	3.59

Luedtke and Landman[5] inferred that floating-bond sites lead to large bond-angle strains including small bond-angles near 60° and 80°. These bond angles near 80° also led to a shoulder in the second peak of $g(r)$ in a-Si models generated with the Stillinger-Weber potential. Hence, the absence of floating bonds in our a-Si film structure considerably relieves the bond-angle strain (Fig. 6).

The distribution of dangling bonds is inhomogeneous in our a-Si layers. All the two-coordinated atoms and a larger density of dangling bonds are near the top surface, where $\sim 59\%$ of the atoms are undercoordinated. The voids in the lower amorphous layers also lead to a higher density of dangling bonds near the amorphous-crystal interface than further into the amorphous layers (Table II).

We have quantitatively characterized the properties of the voids by calculating the structure factor $S(q)$ for wave vectors q parallel to the surface (Fig. 7). A distribution of spherical voids with radius of gyration R_G leads to small wave-vector Guinier scattering given by

$$S(q)=S_0\exp(-q^2R_G^2/3) . \qquad (2)$$

Hence the voids are characterized by an increase in the small wave-vector scattering.

Both the first 13 Å of the $M1$ and $M2$ structures display a rise in $S(q)$ below 1.0 Å^{-1} [Fig. 7(a)], whereas for the next 13 Å a rise in $S(q)$ is only displayed by $M2$ but not $M1$ [Fig. 7(b)]. The larger $S(q)$ at small q for $M2$ suggests there are larger voids in $M2$ than in $M1$. Further, the next 13 Å of $M2$ reveals voids whereas no voids are evident in the corresponding part of $M1$. This was because the adsorbate temperature in the $M1$ simulation was high enough in the later part of the growth to allow for appreciable surface diffusion that prevented voids from forming in the later stages of growth away from the substrate. $M2$ has a potential energy of ~ 0.9 eV/atom higher than the $M1$ structure because of the higher density of voids and consequently dangling bonds in $M2$. This is also consistent with $M2$ having a lower density ($\rho=0.72$) than $M1$ ($\rho=0.85$), in units where the crystal has a density of 1.

The voids in the $M2$ structure have a qualitatively similar structure factor $S(q)$ as those of the bulk a-Si models[13] with voids [Fig. 7(c)], particularly for the small wave-vector scattering. The shift in peak positions in Fig. 7(c) is due to the lower density of the $M2$ film structure than of the bulk model. A radius of gyration, R_G, of 3.6 Å, was extracted from the Guinier plot (Fig. 8) for $M2$. This void radius of gyration is consistent with an

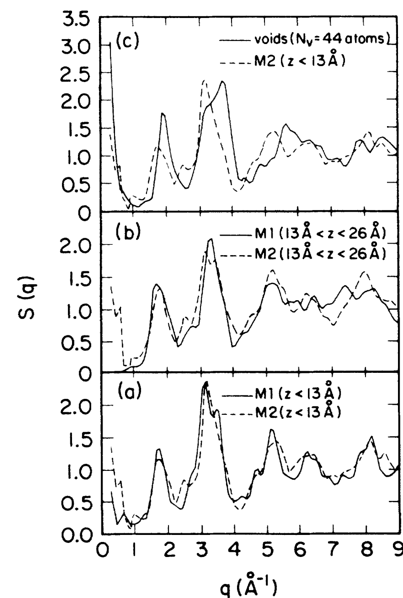

FIG. 7. Static structure factor $S(q)$ for wave vectors q parallel to surface for the lower and the upper layers of the amorphous states produced by cluster deposition [(a) and (b)], compared to the bulk a-Si model with voids (Ref. 13) [(c)].

analysis of the average positions of the atoms. From real-space plots of the projected atom positions as a function of height z we inferred ellipsoidal void shapes, and estimated void radii of 4.0 Å in the x,y plane and 3.2 Å in the z directions, leading to a similar R_G of 3.7 Å.

These results for the void properties are inferred from two separate simulation runs. In another simulation where five clusters were deposited under similar growth conditions, we also observed a void with a spatial extent similar to the $M2$ run. The large amount of cpu time required [$\sim$250 h SCS 40 cpu time] made further full simulations of a-Si film growth unfeasible. We have previously reported[3] the initial stages of cluster-induced growth under a number of initial conditions. We expect that a set of initial conditions different from the $M2$ run would also produce voids with a different location that have a qualitatively similar spatial extent. We do expect the size of the voids to decrease if small clusters are used for the deposition.

With a view of improving the structural quality of the a-Si films we annealed the $M2$ film and studied structural changes. The annealing comprised of equilibrating the $M2$ model at an elevated temperature T_a for 20 000 time steps and then cooling the model at the rate of 0.01 eV per 530 time steps to a cold temperature of 0.03 eV, and a steepest descent relaxation. Two annealing temperatures T_a of 0.12 and 0.20 eV were investigated and resulted in annealed models $A1$ and $A2$, respectively (Table I). Both anneals led to a densification of the structure with densities (ρ) of 0.725 for $A1$ and 0.756 for $A2$, compared with 0.72 for the initial $M2$ structure. The densification was due to the reduction in the number and size of the voids. This interpretation is supported by the Guinier plot (Fig. 8) for the initial 13 Å of the layers, which displays a reduction in the lateral void size from $\sim$3.6 to $\sim$3.1 Å. On the other hand the interfacial voids in both $A2$ and $M2$ appeared very similar. Analysis of the second 13 Å of the deposited layers of $A2$ revealed that the voids in the upper layer of $M2$ had been annealed away as evidenced by the lack of small wave-vector increase in $S(q)$ (Fig. 9).

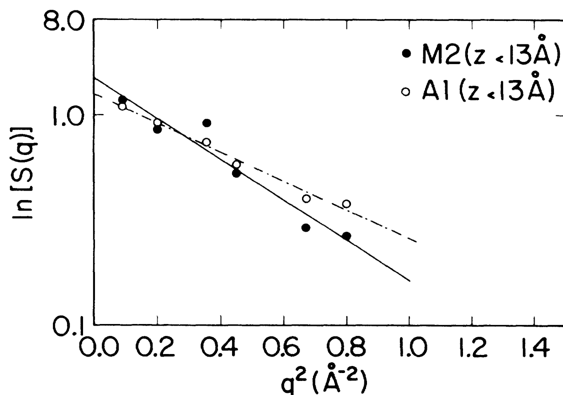

FIG. 8. Guinier plot of the logarithm of the structure factor as a function of q^2 [Eq. (2)]. Only the rapidly increasing $S(q)$ due to scattering from voids for $q < 0.9$ Å^{-1} is shown. The straight lines are drawn by least-squares fitting of the data.

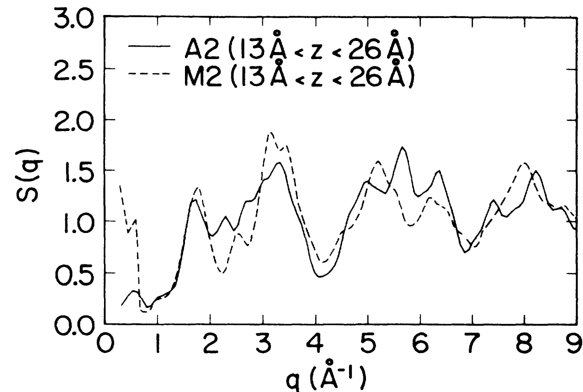

FIG. 9. Static structure factor $S(q)$ for wave vectors q parallel to surface for the annealed a-Si state ($A2$), compared to the original a-Si state ($M2$).

V. EPITAXIAL Si(111) GROWTH SIMULATIONS

In this section we simulate cluster-beam deposition under conditions of high surface diffusivity, which consist of high cluster translational energy ($T_z = 2.1$ and 1.05 eV) together with a moderate substrate temperature ($T_s = 0.12$ eV). These conditions were found in Sec. III (runs 1 and 2, Fig. 1) to lead to a large dissociation of the incident clusters. These cluster kinetic energies are considerably larger than thermal energies and compare well with experimental estimates of cluster energies of 1.0–10.0 eV per atom by Kuiper *et al.*[22]

After deposition of a cluster we allow the system to fully equilibrate by letting it run for a sufficient length of time before depositing the next cluster. Calculations of the spreading index for long times (Fig. 2), indicate that $\eta(t)$ reaches an approximately stationary value after $(28-32)\times 10^3$ time steps (104–118 ps) implying satisfactory equilibration and surface diffusion during this time. We then choose 32×10^3 time steps (118 ps) between deposition of successive clusters. Generally, semiconductors described through three-body or bond-bending interactions, have much longer equilibration times than close-packed metallic systems. The floppy bond-bending modes in covalent systems make energy transfer between atoms much slower than in metals, described through two-body potentials or Lennard-Jones interactions.

The energy deposited by the impinging clusters was dissipated by rescaling the velocities and maintaining at a constant temperature the four Si(111) double layers that formed the initial substrate. Unlike the previous amorphous growth, the adsorbate was not considered in the cooling scheme. As further depositions increased the thickness of the adsorbed layer, the energy relaxation became slower resulting in a gradual warming up of the top surface to about 0.16 to 0.20 eV. This was not a significant problem in the present depositions of 10–13 clusters, but further cluster deposition would probably require cooling some of the deposited species as well.

Cluster-beam deposition at both $T_z = 2.10$ and 1.05 eV resulted in epitaxial growth. In all, 13 and 10 clusters

were deposited corresponding to total simulation times of 1.54 and 1.18 ns for the $T_z=2.10$ and 1.05 eV, runs respectively.

The higher-velocity growth simulation ($T_z=2.1$ eV) produced a uniform array of six-member rings in the deposited layer (Fig. 10) with no five- or eight-member rings that were present in the lower-velocity ($T_z=1.05$ eV) simulation (Fig. 11), emphasizing the importance of having large cluster velocities in the ICB growth process. For $T_z=2.1$ eV, crystalline Si(111) layers were obtained (Fig. 10) with diamondlike stacking in all of the first three deposited double layers. Layers above this were still growing at the end of the simulation. The grown layers have a single domain of diamondlike stacking, in contrast to the two domain structure of the lower-velocity simulation (Fig. 11). Apart from the crystalline six-member rings, two vacancies did persist in both the first and second deposited layers. Filling these vacancies may require annealing times larger than those computationally feasible. The ring statistics, domain structure, and fewer vacancies demonstrated a higher degree of crystalline order in the higher-velocity growth simulation than the simulation at lower cluster velocity.

The $T_z=1.05$ eV growth simulation revealed two domains in the first deposited layer. The lower half of the cell comprised of a domain of wurtzitelike stacking that was separated by a domain wall from a domain of diamondlike stacking in the upper half of the cell (Fig. 11). In the wurtzite stacking the deposited atoms were directly above the substrate atoms. The domain boundary (Fig. 11) consisted of a structure of alternating five- and eight-member rings. This structure is very similar to that proposed for the reconstructed 7×7 Si(111) surface where the wurtzite and diamondlike stackings are observed in either half of the 7×7 unit cell. The proposed structure for the domain boundary in the 7×7 reconstruction has five- and eight-member rings. The second deposited layer also has two domains although the wurtzite stacking domain has decreased in size. There are nine vacancies in the first deposited layer, including a microvoid of five atoms. A significantly greater amount of disorder is present in the second and successively higher layers.

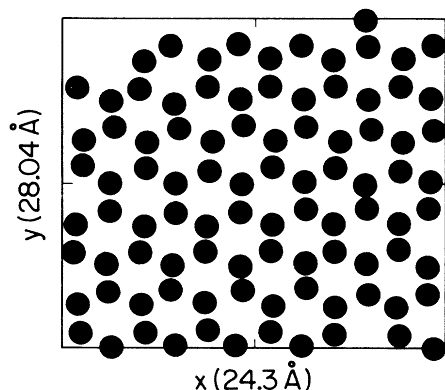

FIG. 10. Projection of the atoms in the first deposited layer using a high cluster translational temperature (T_z) of 2.10 eV and moderate substrate temperature (T_s) of 0.12 eV, demonstrating epitaxial growth with a diamond structure stacking.

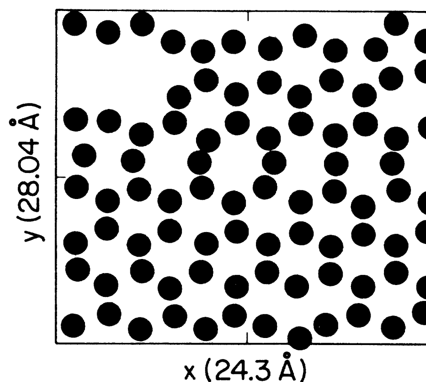

FIG. 11. Projection of the atoms in the first deposited layer using a lower cluster translational temperature (T_z) of 1.05 eV and moderate substrate temperature (T_s) of 0.12 eV. The stacking is wurtzitelike in the lower half and diamondlike in the upper half with a domain wall of five- and eight-member rings separating these two regions.

The occurrence of wurtzite stacking is not surprising since the bulk diamond Si structure is more stable than the bulk wurtzite structure by only 0.015 eV/atom in this Si model at the lattice constant used in the growth simulation. The deposited species may then easily assume either growth orientation.

To compare with other molecular-dynamics simulations of epitaxial Si growth, it is best to normalize deposition rates per surface area, since different size systems were employed in the various cases. Our present simulations utilize a deposition rate of 3.73×10^{-3} ps/atom, in comparison to 3.07×10^{-5} ps/atom by Schneider, Schuller, and Rahman[16] (SSR) for Si(111) and $(8.05-12.08)\times10^{-5}$ ps/atom and Gawlinski and Gunton[17] (GG) for Si(111) growth. The rates used by both SSR and GG are almost 2 orders of magnitude faster than in our present work. This leads us to believe that both the SSR and GG simulations[16,17] led to a molten layer on the substrate with growth proceeding by the movement of the crystal-liquid interface into the liquid phase. This is significantly different from epitaxial thin-film growth, and similar to other simulations of the growth at a crystal-liquid interface.[23,24] We emphasize that in our work we have taken care to avoid the deposited layers becoming molten, by allowing significantly greater equilibration times.

Some difference in the deposition rates here and in the previous simulations arise from the Biswas-Hamann potential in the present work having a slower energy transfer rate than the Stillinger-Weber potential (used by both SSR and GG), as indicated by our earlier studies[3] of the energy transfer rates for single atom depositions with these two Si models. However, the differences in the energy transfer rates probably cannot account for the widely different deposition rates. Comparison of the dynamical properties of different Si-potential models is an aspect for further study.

VI. SUMMARY AND CONCLUSIONS

We have studied the dynamics of cluster deposition on the Si(111) surface and have identified regimes of both low and high surface diffusivity. By utilizing the low surface diffusivity deposition conditions we have simulated the growth of amorphous silicon films on Si(111). The *a*-Si films had a lower density of 0.73–0.84 than of the crystal, and had voids that led to intense small wave-vector scattering in the static structure factor. A remarkable result was that no floating bonds are found in the *a*-Si films, instead all coordination defects comprise of dangling bonds. This directly contrasts with melt-quenched bulk *a*-Si models that have both dangling and floating bonds. Our interpretation is based on the floating bonds being a very mobile species that can easily diffuse with a bond-switching mechanism. Hence, the floating bonds easily diffuse to either the internal void surfaces or external growing surface, where they recombine with the large number of dangling bonds present at these surfaces. Both the lack of floating bonds and the presence of voids lead to lower-band-angle strains in the amorphous films than in the bulk *a*-Si models.

Utilizing conditions of high surface diffusivity in which the impinging clusters dissociate on the surface we have simulated the epitaxial growth on Si(111). A high cluster velocity is necessary for good growth. In our best epitaxial simulations we achieved diamondlike stacking of the deposited atoms while in the other simulation domains of both diamond and wurtzite stacking are found that were separated by a domain wall. We emphasize that our deposition rate was much slower than previous simulations so that a crystal-liquid interface was not allowed to form. We speculate that previous growth simulations, that employed considerably faster deposition rates, had generated a crystal-liquid interface with epitaxy proceeding by a movement of this interface. We tested some single-atom depositions at rates comparable to SSR and found considerable heating at the top surface (with temperatures exceeding the melting temperature) consistent with this idea.

Although the time scales of the simulation are several orders less than experiment, we have shown that the theoretical simulations account well for various short-range relaxation effects involved in epitaxial growth. Long-range diffusion effects are an aspect for further work. Generally, the theoretical trends for the deposition and growth process agree well with experimental data. Another aspect for further study is the vibrational densities of states of these amorphous layers. The melt-quenched models exhibited vibrational densities of states in very good agreement with neutron data, and contained some novel low-frequency localized vibrational modes.[25] The effect of the large number of dangling bonds in the present *a*-Si layers, and an open surface on these localized modes, is an aspect for further study.

ACKNOWLEDGMENTS

R. B. and C. M. S. acknowledge support from the Electronic Power Research Institute (Palo Alto, CA) under Contract No. RP-3070-1. This work was partially supported by a National Science Foundation grant of supercomputer time at the National Center for Supercomputer Applications at the University of Illinois at Urbana-Champaign (Champaign, IL). We also acknowledge support from the U.S. Air Force Office of Scientific Research (Bolling Air Force Base, D.C.). The Ames Laboratory is operated by Iowa State University for the U.S. Department of Energy (U.S. DOE) under Contract No. W-7405-ENG-82 and is supported by the Director for Energy Research, Division of Materials Sciences, Office of Basic Energy Sciences, U.S. DOE.

[1]T. Takagi, *Ion Implantation and Ion Beam Processing of Materials,* edited by G. K. Hubler, O. W. Holland, C. R. Clayton, and C. W. White (North-Holland, New York, 1984), p. 501, and references therein.

[2]J. S. McCalmott, K. M. Lakin, and H. R. Shanks, J. Vac. Sci. Technol. A **5**, 1911 (1987).

[3]R. Biswas, G. S. Grest, and C. M. Soukoulis, Phys. Rev. B **38**, 8154 (1988).

[4]P. C. Kelires and J. Tersoff, Phys. Rev. Lett. **61**, 562 (1988).

[5]W. D. Luedtke and U. Landman, Phys. Rev. B **37**, 4656 (1988); **40**, 1164 (1989).

[6]R. Biswas, G. S. Grest, and C. M. Soukoulis, Phys. Rev. B **36**, 7437 (1987).

[7]M. D. Kluge, J. R. Ray, and A. Rahman, Phys. Rev. B **36**, 4234 (1987).

[8]F. H. Stillinger and T. A. Weber, Phys. Rev. B **31**, 5262 (1985).

[9]J. Tersoff, Phys. Rev. B **37**, 6991 (1988).

[10]R. Biswas and D. R. Hamann, Phys. Rev. B **36**, 6434 (1987).

[11]S. T. Pantelides, Phys. Rev. Lett. **57**, 2979 (1986); **58**, 1344 (1987).

[12]J. C. Phillips, Phys. Rev. Lett. **58**, 2824 (1987); J. C. Phillips, J. C. Bean, B. A. Wilson, and A. Ourmazd, Nature (London) **325**, 121 (1987).

[13]R. Biswas, I. Kwon, A. M. Bouchard, C. M. Soukoulis, and G. S. Grest, Phys. Rev. B **39**, 5101 (1989).

[14]T. A. Postol, C. M. Falco, R. T. Kampwirth, I. K. Schuller, and W. B. Yellon, Phys. Rev. Lett. **45**, 648 (1980).

[15]U. Landman and W. D. Luedtke, Bull. Am. Phys. Soc. **34**, 456 (1989); W. D. Luedtke and U. Landman, Phys. Rev. B **40**, 1164 (1989).

[16]M. Schneider, I. K. Schuller, and A. Rahman, Phys. Rev. B **36**, 1340 (1987).

[17]E. T. Gawlinski and J. D. Gunton, Phys. Rev. B **36**, 4774 (1987).

[18]K. H. Muller, J. Appl. Phys. **61**, 2516 (1987).

[19]K. E. Khor and S. Das Sarma, Chem. Phys. Lett. **134**, 43 (1987), and references therein.

[20]F. Wooten, K. Winer, and D. Weaire, Phys. Rev. Lett. **54**, 1392 (1985); K. Winer, Phys. Rev. B **35**, 2366 (1987).

[21]J. Fortner and J. S. Lannin, Phys. Rev. B **39**, 5527 (1989).

[22]A. Kuiper, G. W. Thomas, and W. J. Schouter, J. Cryst. Growth **51**, 17 (1981).

[23]W. D. Luedtke and U. Landman, Phys. Rev. B **37**, 4647 (1988).

[24]M. Grabow, G. Gilmer, and A. F. Bakker, Mater. Res. Soc. Symp. Proc. **141**, 349 (1988).

[25]R. Biswas, W. A. Kamitakahara, A. Bouchard, C. M. Soukoulis, and G. S. Grest, Phys. Rev. Lett. **60**, 2280 (1988).